conference papers

Structural characterization of *N*-lignoceroyl (C24:0) sphingomyelin bilayer membranes: a re-evaluation

Hiroshi Takahashi,[a]* Tomohiro Hayakawa,[b] Yuko Kawasaki,[c] Kazuki Ito,[d] Tetsuro Fujisawa,[d] Michiko Kodama[c] and Toshihide Kobayashi[b]

[a]Department of Physics, Gunma University, Maebashi 371-8510, Japan, [b]Lipid Biology Laboratory, RIKEN (Institute of Physical and Chemical Research), Wako 351-0198, Japan, [c]Department of Biochemistry, Okayama University of Science, Okayama 700-0005, Japan, and [d]RIKEN Harima Institute/SPring-8, Structural Biochemistry Laboratory, Sayo, Hyogo 679-5148, Japan. Correspondence e-mail: htakahas@fs.aramaki.gunma-u.ac.jp

Sphingomyelin (SM) is a membrane lipid and plays important roles in signaling, protein trafficking, cell growth and death. The structure of the bilayer of a hydrated highly asymmetric SM, *N*-lignoceroyl (C24:0) SM, has been investigated with X-ray diffraction (XRD), simultaneous small-angle X-ray scattering (SAXS), wide-angle XRD and SAXS. At temperatures between two endothermic transitions of hydrated C24:0 SM bilayers, the C24:0 SM formed a ripple phase with the ripple periodicity of ~12–14 nm. At about three months incubation at 277 K, the formation of a stable phase with a short lamellar spacing of 5.62 nm was induced. Based upon the structures revealed by this study and the phase behavior, intermolecular interactions between C24:0 SM molecules in the bilayer membrane are discussed.

1. Introduction

Cells are the minimum unit of life. Phospholipid bilayers are fundamental structural motifs of cell membranes and the membranes of subcellular organelles. Phospholipids are classified into two types, glycerophospholipids and sphingophospholipids, due to a difference of their backbone.

Sphingomyelin (SM) is one of the major sphingolipid components for many animal cell plasma membranes. Recently, it has been reported that SM is involved in various essential biological phenomena. The interaction between SM and cholesterol is believed to be a key factor for the formation of so-called 'lipid rafts' (Ohva-Rekilä *et al.*, 2002). The lipid rafts are lipid microdomains existing in plasma membranes, and play important roles in many biological processes, such as signaling, membrane fusion, lipid sorting, protein trafficking and so on (Simons & Ikonen, 1997). The breakdown of SM by sphingomyelinase results in the formation of ceramide and the ceramide acts as a second messenger involved in cell growth and death (Augé *et al.*, 2000). The studies on the structural and physical properties of SM bilayers are indispensable to understand the molecular mechanism of the biological functions described above.

Naturally occurring SMs are chemically heterogeneous and contain molecular species of asymmetric chain length, *i.e.* the length of the amide-linked acyl chain is frequently longer (22 or 24 C atoms) than that of the sphingosine chain of mostly 18 C atoms (Untrach & Shipley, 1977; Ramstedt *et al.*, 1999; Kodama *et al.*, 2004). Such high asymmetric lipid species are very seldom found in naturally occurring glycerophospholipids, especially for phosphatidylcholine species of animal tissues.

The structure and phase behavior of the most typical asymmetric SM, *N*-lignoceroyl (C24:0) SM, have been investigated by means of various physical methods (Barenholz *et al.*, 1976; Levin *et al.*, 1985; Maulik *et al.*, 1986; Sripada *et al.*, 1987; McIntosh *et al.*, 1992; Maulik

& Shipley, 1995; Bar *et al.*, 1997). Although there is a little discrepancy in the detailed shape of thermograms, all previous differential scanning calorimetry (DSC) studies (Barenholz *et al.*, 1976; Sripada *et al.*, 1987; McIntosh *et al.*, 1992; Maulik & Shipley, 1995; Bar *et al.*, 1997) have reported that hydrated C24:0 SM bilayers exhibit two endothermic phase transitions at ~312 K and at ~317–319 K, *i.e.* there are at least three different phases. As regards the hydrocarbon chain packing mode, a structural model proposed based upon spectroscopic data (Levin *et al.*, 1985) disagrees with that proposed based upon X-ray diffraction (XRD) data (McIntosh *et al.*, 1992; Maulik & Shipley, 1995). It has been reported that various lipids having amide groups in their hydrophobic part exhibit thermal history dependent phase behavior (Koynova & Caffrey, 1995; Takahashi *et al.*, 2005). For the C24:0 SM bilayers, McIntosh *et al.* (1992) have indicated the existence of another stable phase formed by low-temperature incubation. To our knowledge, however, no structural information on the phase has yet been reported.

Using XRD and small-angle X-ray scattering (SAXS), we re-examined the bilayer structures of hydrated C24:0 SM membranes, paying attention to unsolved and controversial points described above. Here, we report that the intermediate temperate phase is not a simple lamellar phase but a ripple phase with a ripple repeat distance of ~12–14 nm and that a long incubation at 277 K induces the formation of another stable phase with a short lamellar spacing of 5.62 nm.

2. Materials and methods

2.1. Sphingomyelin synthesis

N-Lignoceroyl sphingomyelin (*N*-tetracosanoyl sphingomyelin) (C24:0 SM) was produced by semi-synthesis from naturally occurring bovine brain sphingomyelin (BSM), using the deacylation–reacyla-

tion method reported by Sripada et al. (1987). The BSM was obtained from Sigma Co. (St. Louis, MO). Briefly, to produce sphingosyl-phosphocholine (SPC), BSM was dispersed into methanolic HCl solution. The carbon number of sphingosine base of the SPC was predominantly 18 (> 95%), judging from the results of electrospray ionization mass spectrometry (ESI-MS) and nuclear magnetic resonance (NMR) measurements. The condition and analysis method of ESI-MS have been described elsewhere (Kodama et al., 2004). The acylation at the amino group of SPC using lignoceric acid was performed in the presence of dicyclohexylcarbodiimide. Chromatographic purification was repeated until no changes in the temperatures and the widths of the phase transition peaks were observed by DSC. The final purity of the C24:0 SM was shown to be >95% from the results obtained by ESI-MS and NMR. All natural occurring SMs have the D-erythro-(2S,3R) configuration in the sphingosine moiety, however, as pointed out previously (Sripada et al., 1987; Maulik et al., 1991), epimerization of sphingosine does occur during the acid hydrolysis process. The L-threo isomer formation cannot be prevented. The selection by stereoisomers was not performed in this study. Thus, the sample contains ~75% D-erythro SM, and ~25% L-threo isomer.

2.2. Sample preparation

First, the powder sample of C24:0 SM weighted was dispersed into chloroform, and then the solvent was evaporated by nitrogen flow. To remove residue solvent and dehydrate further, the sample was kept under high vacuum (10^{-4} Pa) for more than 8 h. As a result, dried thin lipid films were obtained. Hydrated C24:0 SM samples were prepared by adding desired amounts of distilled water to the dried lipid film samples. To achieve homogeneous hydration, a heating–cooling cycle treatment between 278 K and 343 K was used more than five times. For long time incubation, the sample was stored in a glass tube filled with oxygen-free nitrogen gas to reduce chemical degradation of the sample. Since antibacterial agents were not added, chemical degradation by bacterium might not have been avoided. However, there were not significant differences in the X-ray diffraction patterns between freshly prepared samples and samples incubated at 277 K for about three months, except for additional lamellar peaks with d = ~5.62 nm (Fig. 5), indicating that the sample was not significantly degraded.

2.3. X-ray measurements

Static XRD measurements were carried out at the 15A beamline of the Photon Factory (PF), Tsukuba, Japan (Amemiya et al., 1983), using a short camera length setting to observe higher order lamellar reflections. The PF ring was operated at 2.5 GeV. The wavelength of X-ray beam was 0.150 nm. The sample-to-detector distance was 280 mm and an imaging plate (IP) was used as the detector. The digitization of the IP data was performed with a BAS2000 system (Fuji Photo Film Co. Ltd, Tokyo). Typical exposure time was 180 s.

Temperature-scan simultaneous SAXS and wide-angle X-ray diffraction (WAXD) measurements were performed at the 9C beamline of PF, with a wavelength of 0.150 nm. At the beamline, SAXS and WAXD data were collected simultaneously using two position sensitive proportional counters (Abe & Takahashi, 2003). The sample-to-detector distances were about ~1000 mm and ~280 mm for SAXS and WAXD, respectively. The sample temperatures were controlled using a FP84 differential scanning calorimeter (Mettler–Toledo K.K.); however, in the present study, DSC signals were not recorded. The apparatus was set up for X-ray measurements according to Takahashi et al. (1995).

SAXS measurements for dilute samples were carried out at RIKEN Structural Biology Beamline I (BL45XU) (Fujisawa et al., 2000) at SPring-8 (Hyogo, Japan) with an 8 GeV synchrotron radiation source. The X-ray wavelength used was 0.09 nm and the beam size at the sample position was ~0.4 × 0.7 mm². The sample-to-detector distance was 840 mm. The sample temperature was controlled with a thermoelectric device. Typical exposure time was 10 s. SAXS data were recorded with a large-aperture (150 mm diameter) TV-type detector consisting of a beryllium-windowed X-ray image intensifier and a charge-coupled device (CCD) image sensor (Hamamatsu Photonics, Japan) (Amemiya et al., 1995). The image distortion and non-uniform response of the detector were corrected according to Ito et al. (2005).

The reciprocal spacing (S), $S = 1/d = (2/\lambda)\sin\theta$ (where d is the lattice spacing, 2θ is the scattering angle, and λ is the wavelength of the X-rays), was calibrated with silver behenate (Blanton et al., 1995). Water scattering profile was also measured in order to subtract the background. Two-dimensional data on both the IP and CCD X-ray detector were transformed into one-dimensional data by radial integration with FIT2D software written by Dr A. Hammersley (http://www.esrf.fr/computing/scientific/FIT2D/).

3. Results

3.1. Static XRD

In order to characterize the structures of each phase of C24:0 SM bilayers, XRD profiles were recorded at three different temperature regions: 283 K, ~313–318 K and 333 K. Several samples containing different amounts of water were examined to reconstruct electron density profiles from observed lamellar diffraction intensity data by using s so-called swelling method. Here, we express water content by a water/lipid molar ratio, N_w, and studied the samples with the hydration range from N_w = 10 (~18 wt% H$_2$O) to N_w = 40 (~47 wt% H$_2$O).

At 283 K and 333 K, series of diffraction peaks with the reciprocal spacing (S) ratio of 1:2:3... were observed for all hydration levels examined here, indicating that hydrated C24:0 SM bilayers form a lamellar structure at both temperatures. The observed lamellar spacing values were changed depending on N_w. The ranges were 6.45–6.86 nm and 6.06−7.28 nm for 283 K and 333 K, respectively. The observed XRD intensities were corrected for the Lorentz factors, normalized, and converted to the magnitude of structure factors according to Worthington & Blaurock (1969). Phases of each diffraction peak were determined from the analysis of the swelling XRD data sets, using the Shannon sampling theorem (Sayre, 1952, Fig. 1). The values of structure factor at S = 0 were estimated by a method proposed by King & Worthington (1971).

Fig. 2 shows relative electron density profiles of C24:0 SM bilayers at 283 K and 333 K. These profiles are almost identical with those reported previously (McIntosh et al., 1992; Maulik & Shipley, 1995). The two highest peaks in each profile are assigned to the electron-rich phosphate headgroups of C24:0 SM molecules. The distances are slightly varied by the water content. The values are in the range of ~5.2–5.3 nm and ~4.4–4.8 nm for 283 K and 333 K, respectively.

For ~313–318 K, several diffraction peaks with a shoulder were observed. This indicates that C24:0 SM bilayers do not form a simple one-dimensional lamellar lattice at temperatures between two endothermic phase transitions. This result is not consistent with that of Maulik & Shipley (1995). This problem will treated in the next section.
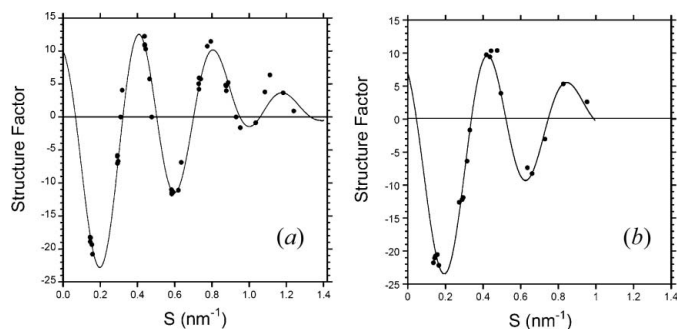
Figure 1
Plots of the normalized structure factor for C24:0 SM at (*a*) 283 K and (*b*) 333 K as a function of reciprocal space (*S*). Curves correspond to the continuous Fourier transform calculated using the Shannon sampling theorem.

3.2. Temperature-scan SAXS/WAXD

Structural changes during heating were investigated with temperature-scan SAXS/WAXD measurements. The heating scan rate was 2 K min^{-1}. Fig. 3 shows the result for a sample of N_w = 40. For both SAXS and WAXD data, it can be recognized that two structural change events take place, corresponding to two endothermic phase transitions.

In SAXS region [Fig. 3(*a*)], the positions of the strong peak observed around S = 0.10–0.15 nm^{-1} are changed at ~310 K and ~319 K. With increasing temperature, a sharp WAXD peak at S = 2.39 nm^{-1} (d = 0.418 nm) disappears, indicating that the hydrocarbon chains are melted at above ~319 K. The width of the WAXD peak is slightly broader at ~310 K. In the temperature range from ~ 310 K to ~319 K, the peak observed at S = ~0.10 nm^{-1} has a shoulder on the wider angle side. The existence of relatively large water region between each adjoining bilayer would provide a space for large thermal fluctuation. Owing to this fluctuation, diffraction peaks are not well resolved. Thereby, we cannot get further detailed information.

In order to get a sharp diffraction profile, we next investigated samples containing less water. Fig. 4 represents the data for an N_w =
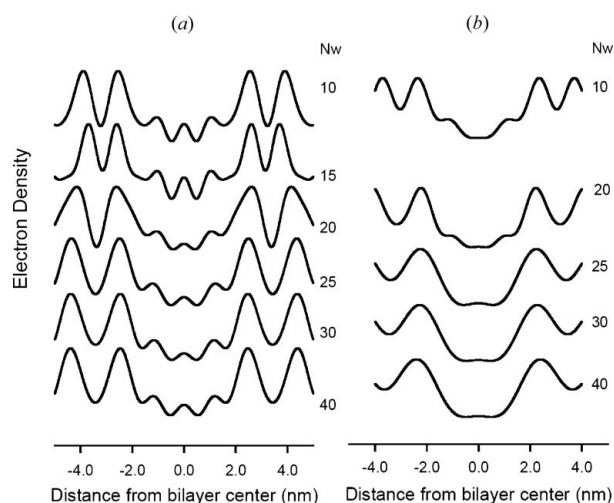
10 sample. Agreeing with previous DSC study (Maulik & Shipley, 1995), the phase transition temperatures where structural changes are observed, increase in comparison with the N_w = 40 sample (Fig. 4). In addition to a strong peak at S = ~0.15 nm^{-1}, at temperatures between 316 K and 321 K, two weak but distinct diffraction peaks appear at S = ~0.07–0.08 nm^{-1} (d = ~12–14 nm) and S = ~0.18 nm^{-1} (d = ~5.6 nm). These three diffraction peaks can be indexed as the 01, 10, 11 reflections of a two-dimensional monoclinic lattice. From the spacings of those peaks, for example, at 319.5 K, the lattice parameters are calculated to be a = 6.61 nm, b = 13.6 nm and γ = 101.8°. Judging from the value (d = ~12–14 nm), the spacing of the 01 peak corresponds to the periodic repeat distance of a ripple structure. That is, we conclude that the C24:0 SM bilayers with N_w = 10 are in a ripple phase at the temperatures between two endotherms.

3.3. SAXS of dilute samples

McIntosh *et al.* (1992) have reported thermal history dependent phase behavior of C24:0 bilayers. By DSC, they have found that a sample kept at 273 K for six days exhibits a slightly higher (~0.1 K) peak temperature and about 1.5× larger transition enthalpy value for the low-temperature transition, compared with the second heating scan after cooling from the temperature above the high-temperature transition, whereas the peak temperature and enthalpy values for the high-temperature transition are unchanged. This suggests the exis-
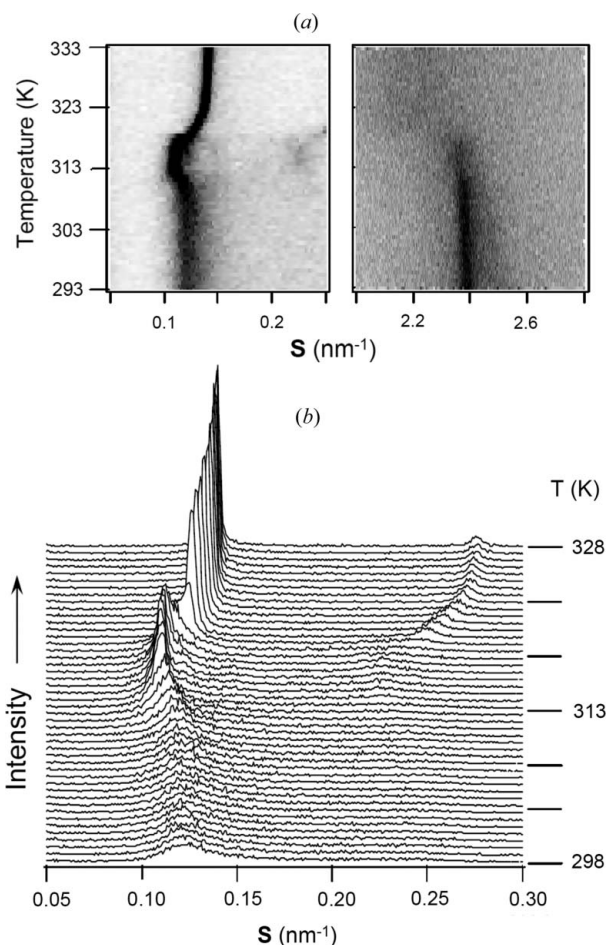

Figure 2
Electron density profiles for C24:0 SM bilayers at (*a*) 283 K and (*b*) 333 K. Arbitrary scale. The water/lipid molar ratios, N_w, of the samples are indicated on the right-hand side of each profile.
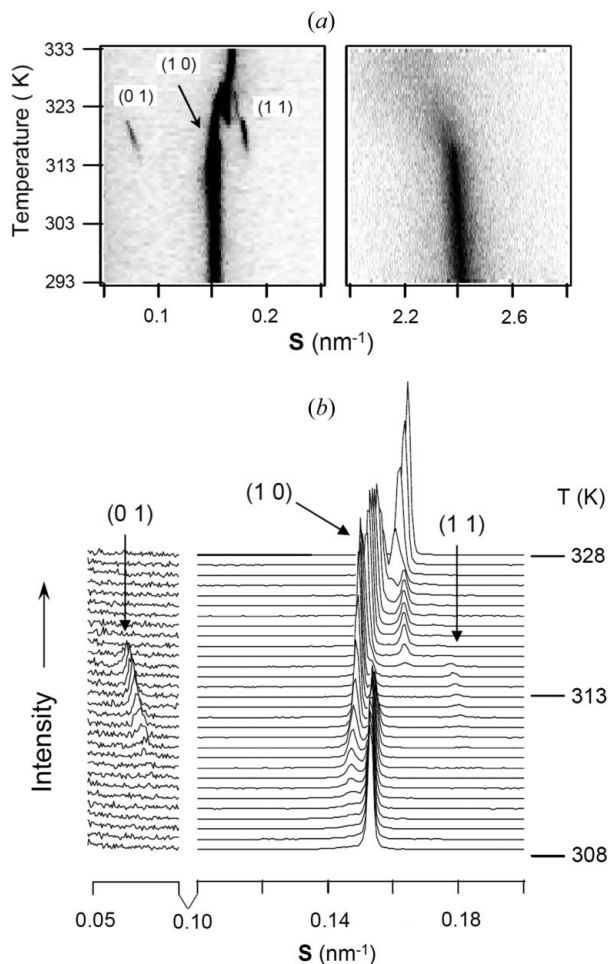
Figure 3
(*a*) Gray-level plot of SAXS/WAXD intensities as a function of temperature for C24:0 SM bilayers of N_w = 40 during a heating scan at a rate of 2 K min^{-1}. The darker areas represent higher intensities. (*b*) Stack plot of the SAXS data of (*a*).

Figure 4
(a) Gray-level plot of SAXS/WAXD intensities as a function of temperature for C24:0 SM bilayers of $N_w = 10$ during a heating scan at a rate of 2 K min^{-1}. The darker areas represent higher intensities. (b) Stack plot of the SAXS data of (a). To recognize a weak diffraction peak easily, the scattering intensity scale is expanded by ten times for the region of $S = 0.05$–0.10 nm^{-1}.

tence of another stable gel phase. From a structural viewpoint, we explored this problem.

The detailed lipid concentration condition is not given in the paper by McIntosh *et al.* (1992). Judging from the fact that they used a high-resolution MicroCal DSC instrument, the lipid concentration should be much lower than that used in the above measurements of the present study. In addition, our DSC study suggested that the change of the transition enthalpy value induced by keeping the sample at low temperatures depends on the lipid concentration, *i.e.* the enthalpy change value is extremely small for high lipid concentration samples (manuscript in preparation). Taking these matters into consideration, we decided to examine a sample of $N_w = \sim1000$ ($\sim$95 wt% water).

Fig. 5 presents SAXS profiles for the dilute C24:0 SM bilayer sample recorded at various temperatures. At 293 K, in addition to typical quasi-Bragg peak scattering from weakly ordered bilayer membrane stacks (Pabst *et al.*, 2003), a relatively sharp peak is observed at $S = 0.178$ nm^{-1} ($d = 5.62$ nm). The intensity of this peak decreases with increasing temperature and disappears at 313 K. Above the chain melting transition, sharp diffraction peaks are observed, indicating that the correlation between adjoining bilayers becomes stronger in a liquid crystalline phase. After cooling, the peak observed at $S = 0.178$ nm^{-1} ($d = 5.62$ nm) initially is not observed and
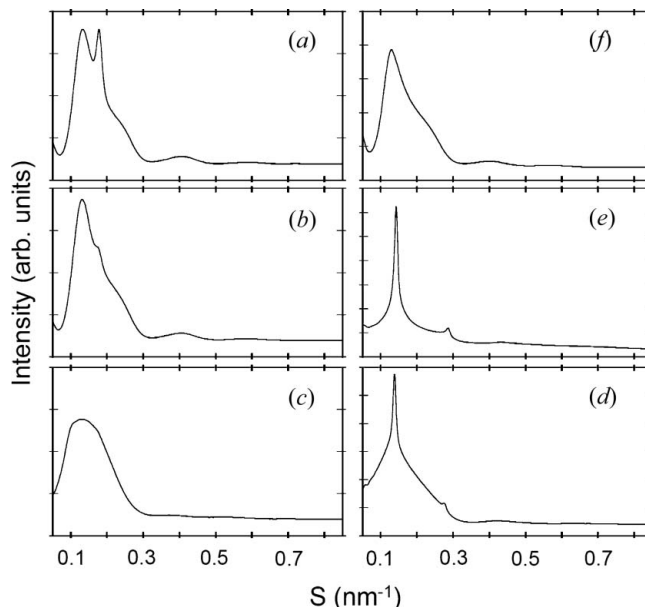

Figure 5
SAXS profiles for dilute C24:0 SM sample, $N_w = \sim1000$ kept at 277 K for about three months, recorded at (a) 293 K, (b) 303 K, (c) 313 K, (d) 323 K, (e) 333 K and (f) 293 K cooling from 333 K. Arbitrary scale.

only a broad quasi-Bragg peak scattering profile is detected. Hence, it can be concluded the relatively sharp peak with a short spacing of 5.62 nm is reflected from a stable phase induced by low-temperature incubation.

To get further information, we subtracted the SAXS profile recorded after cooling [Fig. 5(d)] from initial SAXS profile recorded at 293 K [Fig. 5(a)]. Fig. 6 shows the difference profile obtained by the subtraction. It can be seen that there are four weak but relatively sharp diffraction peaks in addition to the peak at $S = 0.178$ nm^{-1}. The spacing ratio of these peaks is 1/1: 1/2: 1/3: 1:4, inferring that the C24:0 SM molecular assembly in the stable phase transformed by low-temperature incubation forms a lamellar structure with the periodicity of 5.62 nm.

4. Discussion

The main new results of this study are: (1) the C24:0 SM bilayers form a ripple phase at temperatures between the two endotherms; (2) the
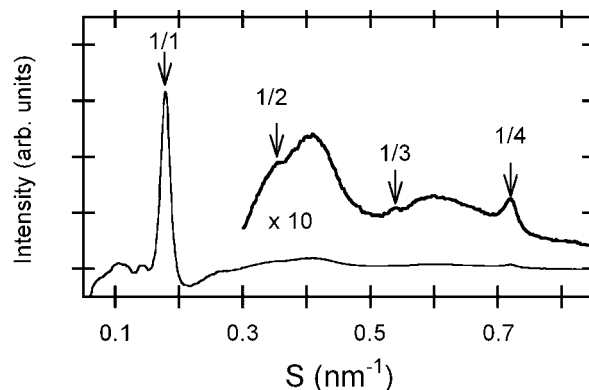

Figure 6
The pattern calculated by subtraction of the SAXS profile recorded after cooling [Fig. 5(d)] from the initial SAXS profile recorded at 293 K [Fig. 5(a)]. The upper plot shows a tenfold vertical scale expansion of the lower plot.

formation of a stable lamellar phase with a relatively shorter repeat spacing is induced by long incubation at low temperature. Regarding the first result, Bar *et al.* (1997) have speculated the possibility from analogy with BSM bilayers that have been revealed to form a ripple phase by freeze-fracture electron micrographic observation (Hui *et al.*, 1980). The present study gives clear experimental evidence of ripple phase formation for C24:0 SM bilayers. Regarding the second result, the existence of another stable phase has been suggested from DSC studies (McIntosh *et al.*, 1992). In addition to confirming the stable phase formation, we could determine the lamellar repeat spacing.

Based on the present results and literature data, we propose the model of structural changes of hydrated C24:0 SM bilayers in heating (Fig. 7). In agreement with previous studies (McIntosh *et al.*, 1992; Maulik & Shipley, 1995), the electron density profiles at 283 K and 333 K (Fig. 2) contain a relatively flat region around the geometric center of the bilayers. This characteristic shape indicates that terminal methyl groups of the C24:0 SM molecules are not localized in the geometric center of the bilayers. Further taking account of the short distance between two highest peaks of electron density profiles, which corresponds to bilayer thickness, it is very likely that the C24:0 SM bilayers form a partially interdigitated structure at both 283 K and 333 K (Fig. 7). We come to the same conclusion as McIntosh *et al.* (1992) and Maulik & Shipley (1995), that in the structure, 24-carbon long acyl chains in one monolayer cross the bilayer center and oppose the shorter 18-carbon sphingosine chains from the other monolayer.

From the conclusion that, in both low- and high-temperature phases, the hydrocarbon chains of C24:0 SM bilayers are packed into a partially interdigitated structure, it is natural to assume that a partially interdigitated structure is also formed in the ripple phase that appeared at the intermediate temperature region (Fig. 7).

For asymmetric phosphatidylcholines (PCs), it has been reported that there are two different types of interdigitated structures: mixed-chain and partially interdigitated packing structures. In the mixed-chain interdigitated structure, the long acyl chain spans the whole width of the bilayer's hydrocarbon core and the shorter chains, each from a lipid molecule in the opposing leaflet, meet end to end in the bilayer midline. For asymmetric PCs, the formation of a ripple phase has been revealed by SAXS (Cunningham *et al.*, 1998). To our knowledge, all asymmetric PCs having a ripple phase exhibit a partially interdigitated gel phase below the ripple phase, whereas the mixed-chain interdigitated gel phase of highly asymmetric PCs converts directly into a lamellar liquid crystalline phase in heating (see Huang *et al.*, 1993, and others cited therein). This fact also supports our proposal (Fig. 7).

The transition enthalpy value from a lamellar gel phase to a ripple phase is generally one fourth to one fifth of that from the ripple phase

to a liquid crystalline phase for both symmetric and asymmetric PCs (see *LIPIDAT*, http://www.lipidat.chemistry.ohio-state.edu). Many theoretical and experimental studies (see Heimburg, 2000, and others cited therein) have suggested that the transition enthalpy value from a lamellar gel phase to a ripple phase of PC bilayers originates from the chain melting taking place in a small part of the hydrocarbon chains of PC bilayers or small number of PCs in the bilayers. On the other hand, the enthalpy of the low-temperature gel-to-ripple phase transition of C24:0 SM bilayers is relatively greater and its value is about two thirds of that of the high-temperature chain-melting transition (Sripada *et al.*, 1987; McIntosh *et al.*, 1992; Maulik & Shipley, 1995). Judging from the WAXD profiles (Figs. 3 and 4), only small parts of the hydrocarbon chains are melted in the partially interdigitated ripple phase. Hence, it is likely that another factor also contributes the large transition enthalpy value. Depending on their chemical structures, sphingolipids act as both acceptor and donor of hydrogen bond, whereas glycerolipids act only as hydrogen-bond acceptor (Barenholz & Thompson, 1999; Ramstedt & Slotte, 2002). This nature leads to the idea of the existence of a hydrogen-bond network between the SM molecules in the bilayers, where hydrogen bonds are formed between the hydroxyl and amide groups of the ceramide moiety of SM, and the phosphate headgroup and hydroxyl groups of the ceramide moiety (Masserini & Ravasi, 2001). Recent computer simulation studies (Chui *et al.*, 2003; Mombelli *et al.*, 2003) have suggested the formation of a hydrogen-bond network in SM bilayers. Thus, we speculate that with increasing temperature, breakdown of the hydrogen-bond network takes place in parts, resulting in the relatively large enthalpy change.

Spectroscopic studies of C24:0 SM bilayers (Levin *et al.*, 1985) have suggested the presence of both mixed-chain and partially interdigitated gel phases. The bilayer thickness of mixed-chain interdigitated structures is shorter than that of partially interdigitated structures. Judging from the short lamellar spacing (5.62 nm), C24:0 bilayers in the stable phase observed after incubation might form a mixed-chain interdigitated structure. We cannot, however, exclude the possibility of a partially interdigitated structure with an extremely tilted chain packing. Further detailed structural investigations are required.
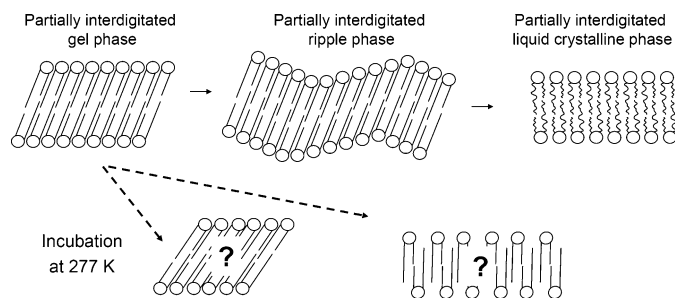
Figure 7
Schematic representation of structural change of C24:0 SM bilayers in heating scan.

References

Abe, S. & Takahashi, H. (2003). *J. Appl. Cryst.* **36**, 515–519.
Amemiya, Y., Ito, K., Yagi, N., Asano, Y., Wakabayashi, K., Ueki, T. & Endo, T. (1995). *Rev. Sci. Instrum.* **66**, 2290–2294.
Amemiya, Y., Wakabayashi, K., Hamanaka, T., Wakabayashi, T., Matsushita, T. & Hashizume, H. (1983). *Nucl. Instrum. Methods*, **208**, 471–477.
Augé, N., Nègre-Salvayre, A., Salvayre, R. & Levade, T. (2000). *Prog. Lipid Res.* **39**, 207–229.
Bar, L. K., Barenholz, Y. & Thompson, T. E. (1997). *Biochemistry*, **36**, 2507–2516.
Barenholz, Y., Suurkuusk, J., Mountcastle, D., Thompson, T. E. & Biltonen, R. L. (1976). *Biochemistry*, **15**, 2441–2447.
Barenholz, Y. & Thompson, T. E. (1999). *Chem. Phys. Lipids*, **102**, 29–34.
Blanton, T. N., Huang, T. C., Toraya, H., Hubbard, C. R., Robie, S. B., Louer, D., Gobel, H. E., Will, G., Gilles, R. & Raftery, T. (1995). *Powder Diffr.* **10**, 91–95.

Chui, S. W., Vasudevan, S., Jakobsson, E., Mashl, R. J. & Scott, H. L. (2003). *Biophys. J.* **85**, 3624–3635.

Cunningham, B. A., Brown, A. D., Wolfe, D. H., Williams, W. P. & Brain, A. (1998). *Phys. Rev. E*, **58**, 3662–3672.

Fujisawa, T., Inoue, K., Oka, T., Iwamoto, H., Uraga, T., Kumasaka, T., Inoko, Y., Yagi, N., Yamamoto, M. & Ueki, T. (2000). *J. Appl. Cryst.* **33**, 797–800.

Heimburg, T. (2000). *Biophys. J.* **78**, 1154–1165.

Huang, C., Wang, Z.-Q., Lin, H.-N. & Brumbaugh, E. (1993). *Biochim. Biophys. Acta*, **1145**, 298–310.

Hui, S. W., Stewart, T. P. & Yeagle, P. L. (1980). *Biochim. Biophys. Acta*, **601**, 271–281.

Ito, K., Kamikubo, H., Yagi, N. & Amemiya, Y. (2005). *Jpn. J. Appl. Phys.* **44**, 8684–8691.

King, G. I. & Worthington, C. R. (1971). *Phys. Lett. A*, **35**, 259–260.

Kodama, M., Abe, M., Kawasahi, Y., Hayashi, K., Ohira, S., Nozaki, H., Katagiri, C., Inoue, K. & Takahashi, H. (2004). *Thermochim. Acta*, **416**, 106–111.

Koynova, R. & Caffrey, M. (1995). *Biochim. Biophys. Acta*, **1255**, 213–236.

Levin, I. W., Thompson, T. E., Barenholz, Y. & Huang, C. (1985). *Biochemistry*, **24**, 6282–6286.

McIntosh, T. J., Simon, S. A., Needham, D. & Huang, C. H. (1992). *Biochemistry*, **31**, 2012–2020.

Masserini, M. & Ravasi, D. (2001). *Biochim. Biophys. Acta*, **1532**, 149–161.

Maulik, P. R., Atkinson, D. & Shipley, G. G. (1986). *Biophys. J.* **50**, 1071–1077.

Maulik, P. R. & Shipley, G. G. (1995). *Biophys. J.* **69**, 1909–1916.

Maulik, P. R., Sripada, P. K. & Shipley, G. G. (1991). *Biochim. Biophys. Acta*, **1062**, 211–219.

Mombelli, E., Morris, R., Taylor, W. & Fraternali, F. (2003). *Biophys. J.* **84**, 1507–1517.

Ohva-Rekilä, H., Ramstedt, B., Leppimäki, P. & Slotte, J. P. (2002). *Prog. Lipid Res.* **41**, 66–97.

Pabst, G., Koschuch, R., Poza-Navas, B., Rappolt, M., Lohner, K. & Laggner, P. (2003). *J. Appl. Cryst.* **36**, 1378–1388.

Ramstedt, B., Leppimäki, P., Axberg, M. & Slotte, J. P. (1999). *Eur. J. Biochem.* **266**, 997–1002.

Ramstedt, B. & Slotte, J. P. (2002). *FEBS Lett.* **531**, 33–37.

Sayre, D. (1952). *Acta Cryst.* **5**, 843.

Simons, K. & Ikonen, E. (1997). *Nature*, **387**, 569–572.

Sripada, P. K., Maulik, P. R., Hamilton, J. A. & Shipley, G. G. (1987). *J. Lipid Res.* **28**, 710–718.

Takahashi, H., Matuoka, S., Amemiya, Y. & Hatta, I. (1995). *Chem. Phys. Lipids*, **76**, 115–121.

Takahashi, H., Okumura, Y. & Sunamoto, J. (2005). *Biochim. Biophys. Acta*, **1713**, 40–50.

Untrach, S. H. & Shipley, G. G. (1977). *J. Biol. Chem.* **252**, 4449–4457.

Worthington, C. R. & Blaurock, A. E. (1969). *Biophys. J.* **9**, 970–990.